Chemical Science

ROYAL SOCIETY OF CHEMISTRY

EDGE ARTICLE

View Article Online
View Journal | View Issue

Check for updates

Cite this: *Chem. Sci.*, 2022, **13**, 1037

All publication charges for this article have been paid for by the Royal Society of Chemistry

Received 7th August 2021
Accepted 21st December 2021

DOI: 10.1039/d1sc04341b

rsc.li/chemical-science

Polariton ring currents and circular dichroism of Mg-porphyrin in a chiral cavity†

Shichao Sun, Bing Gu and Shaul Mukamel *

By placing Mg-porphyrin molecules in a chiral optical cavity, time reversal symmetry is broken, and polariton ring currents can be generated with linearly polarized light, resulting in a circular dichroism signal. Since the electronic state degeneracy in the molecule is lifted by the formation of chiral polaritons, this signal is one order of magnitude stronger than the bare molecule signal induced by circularly polarized light. Enantiomer-selective photochemical processes in chiral optical cavities is an intriguing future possibility.

Introduction

Optical cavities have recently emerged as a new means for manipulating photophysical and photochemical molecular processes.[1–3] The vacuum electric field due to the zero-point energy of a confined optical cavity mode can modify the molecular potential energy landscape even in the absence of external driving fields. The cavity mode can be characterised by the qualify factor Q, defined as the ratio of the cavity frequency and resonance width. Larger Q implies higher quality and longer cavity photon lifetime. Substantial couplings can be induced between electronic or vibrational molecular transitions and the confined cavity mode. In the strong coupling regime whereby the light-matter coupling is stronger than the loss rate of the cavity mode and the molecular decoherence rate, the molecular degrees of freedom mix with the cavity photon to form hybrid light-matter states, known as polaritons. Molecular polaritons, which carry both characters of matter and light, have been reported for a plethora of systems, even for a single molecule.[3–8] Experimental evidence suggesting that the strong coupling can alter the branching ratio of a chemical reaction,[9] induce long-range energy transfer,[4,5] enhance Raman scattering,[7] and modify photochemical reaction rates[10] has triggered extensive theoretical activities.[10–30]

Chiral cavities refer to optical cavities with spatial, temporal or spatio-temporal symmetries broken.[31] Here we focus on the chiral cavity whose mode profile depend on the circular polarization. They offer a new means for controlling photophysical properties of molecules. Such chiral optical cavity can be constructed by embedding the Faraday rotator[32] in a Fabry–Perot cavity.[31] Faraday rotator is a material with magneto-optical effect. With a longitudinal static magnetic field is applied on the Faraday rotator, the left and right circularly polarized light are shifted by different phases when transmitting through it. The phase of the circularly polarized standing wave formed in the cavity is shifted by the Faraday rotator. This can lead to an asymmetry in the spatial profiles of the left and right circularly polarized cavity mode, in contrast to non-chiral cavities where the spatial profile is independent of the polarization. By tuning the phase shift, it is possible to position the spatial envelope peak of the right circularly polarized wave at the node of the left circularly polarized wave. We can then create regions in the cavity where thin layers are sorely subjected to the left or right circularly polarized cavity mode, as shown in Fig. 1. Such chiral cavity where left and right circularly polarized cavity modes couples differently to the embedded molecules is highly promising for controlling the chiral photophysical properties of molecules and materials. A characteristic feature of chiral cavities is that it breaks the time reversal symmetry. Time reversal symmetry is a property where physical property is invariant under time reversal operation. For a cavity with regular mirrors, time reversal symmetry cannot be broken. At a given location, a time reversal operation will revert a circular polarization mode to the opposite circular polarization. With time reversal symmetry, an embedded molecule will effectively couple with a linearly polarization mode in a non-chiral cavity. Breaking this symmetry can lead to interesting effects such as light induced ring currents,[33] magnetic circular dichroism[44] and topological states.[61]

In this paper, we explore the effects of time reversal symmetry breaking on Mg-porphyrin molecules placed in a chiral cavity.

The first effect is an induced ring current in a cyclic conjugated molecule. In the absence of external perturbations, ring currents of opposite directions are equally likely, and no net current is produced. By breaking time reversal symmetry using either circularly polarized light[33–36] or a static magnetic field,[37–42] ring current in one direction is favored and a net ring current can be produced. The two methods have different features. The

Department of Chemistry and Department of Physics & Astronomy, University of California, Irvine, USA. E-mail: smukamel@uci.edu

† Electronic supplementary information (ESI) available. See DOI: 10.1039/d1sc04341b

Open Access Article. Published on 03 enero 2022. Downloaded on 20/12/2025 09:30:08 a. m..
This article is licensed under a Creative Commons Attribution-NonCommercial 3.0 Unported Licence.

Open Access Article. Published on 03 enero 2022. Downloaded on 20/12/2025 09:30:08 a. m..
This article is licensed under a Creative Commons Attribution-NonCommercial 3.0 Unported Licence.

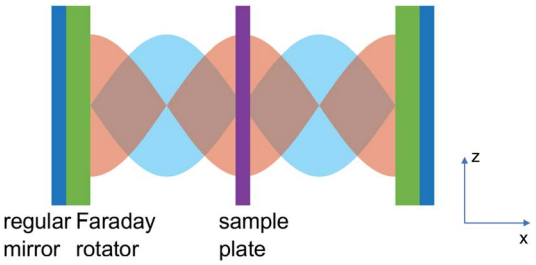

Fig. 1 Optical chiral cavity created by Faraday rotator and regular mirrors. Two Faraday rotators (green) are placed on the interior side of the two mirrors (blue). A magnetic field is applied along the cavity x-axis. The left circularly polarized standing wave (light blue) and right circularly polarized standing wave (orange) have a phase difference. At the node of the left circularly polarized standing wave, the right circularly polarized wave dominates. A plate of sample molecules is placed in the plane at the peak of right circularly polarized standing wave.

static magnetic field perturbs all states since it is not resonant with any excited state, whereas circularly polarized light can be tuned to be resonant with a selected state. Another difference is that circularly polarized light does not lift the degeneracy of excited states while a magnetic field does. In an achiral molecule with a C_n rotation axis where $n > 2$ pumped with circularly polarized pulse, the time-resolved circular dichroism (CD) signal involving doubly degenerate states with E character is usually weak since CD signals from a pair of doubly degenerate states cancel out.[43] We refer to doubly degenerate states as E states in the following. The magnetic field, in contrast, removes the E states degeneracy and produces two relatively strong peaks with opposite sign in the magnetic circular dichroism (MCD) signal, known as $\mathcal{A}$-term in MCD spectrum.[43–45]

Chiral optical cavities breaks the time-reversal symmetry through the vacuum field with local optical chirality. The cavity mode frequency can be tuned by changing the distance between mirrors to couple with selected molecular excited states. By placing the Mg-porphyrin molecules in a chiral optical cavity, a ring current can be created even by a linearly polarized light, in contrast to a bare molecule, which requires a circularly polarized light pulse to break the time reversal symmetry. Moreover, the cavity mode selectively couples with one of the degenerate pair of E states of a molecule possessing a rotation axis C_n ($n > 2$). This lifts the two fold degeneracy thus producing a stronger CD signal.

Hereafter, we explore the effects of chiral optical cavity on the polariton ring currents. It is well established computationally that a circular polarized light pulse can create a ring current in Mg-porphyrin.[33] This is formed by the coherence of degenerate excited states with E_u irreducible representation of Mg-porphyrin and can be detected by time-resolved X-ray circular dichroism.[46] Here, we show how to create a ring current by applying a linearly polarized pump pulse on a Mg-porphyrin molecule placed in a chiral optical cavity. Extending the work in ref. 46, we probe the polariton ring current by measuring the UV-visible circular dichroism signal following optical pump excitation. We further explore the enhancement of the CD signal in the chiral cavity by lifting the excited state degeneracy and the signatures of detuning and coupling strength of the chiral cavity. Finally, we compare the polariton CD with molecular MCD, and show that they share a similar mechanism of enhancing the CD signal.

Theory and methodology

As shown in Fig. 1, we place the molecules in the y–z plane, with the four N atoms lying along the y, z axes. The molecular geometry is optimized using DFT with the B3LYP functional[47–50] and the 6-31g(d) basis set and Gaussian 16.[51] The excited states are computed with time-dependent density functional theory in the Tamm–Dancoff approximation (TDA) using the Chronus Quantum code.[52] Both DFT and TDA calculations employ the same density functional and basis set used in the geometry optimization. The energy and transition electric dipoles between the ground and excited states are listed in Table S1 in ESI.† The transition dipole moments between excited states are given in Table S2.†

The molecular excited states $|m_1\rangle$ and $|m_2\rangle$ are degenerate with energy $\hbar\omega_1 = 2.4481$ eV, and have transition electric dipoles along z and $-y$ respectively. We construct their linear combinations

$$|m_\pm\rangle = \frac{1}{\sqrt{2}}(-|m_2\rangle \pm i|m_1\rangle) \quad (1)$$

whose energies $\hbar\omega_\pm$ are the same as $\hbar\omega_1$ and $\hbar\omega_2$. The $|m_\pm\rangle$ states carry molecular ring currents around x-axis with opposite directions.[33] The bare molecular Hamiltonian is

$$H_{mol} = \hbar\omega_g|g\rangle\langle g| + \sum_j \hbar\omega_j|m_j\rangle\langle m_j| \quad (2)$$

where $|g\rangle$ is the molecular ground state. $|m_j\rangle$ runs over the ring current carrying molecular excited states $j = +, -$ and higher excited states $j = 3, 4, 5\ldots$.

The chiral cavity can be built with two Faraday mirrors placed in the yz plane (Fig. 1). Unlike ordinary (Fabry–Perot) cavities which contain two regular mirrors, a chiral cavity is formed with two parallel Faraday mirrors, where a Faraday rotator is placed on top of each regular mirror. A circularly-polarized light reflected by a regular mirror has the reverse circular polarization and propagation direction, thus forming a circularly polarized standing wave. In a cavity with regular mirrors, due to time reversal symmetry, the coexistence of standing wave modes with opposite circular polarization makes the cavity mode achiral. In a chiral cavity, the Faraday rotator rotates the polarization of the left/right circularly polarized standing wave differently, giving their spatial envelope a phase difference φ (see eqn (S3) in ESI†). For $\varphi = \frac{\pi}{2}(2n+1)$ where $n = 0, 1, 2\ldots$, the peak of the spatial envelope of right circularly polarized wave lies at the node of the left circularly polarized wave, producing a plane dominated by a right circularly polarized wave (Fig. 1) where a Mg-porphyrin thin film is placed. The cavity-mode frequency is $\hbar\omega_c = \hbar\omega_+ - \delta$, where δ is its detuning.

© 2022 The Author(s). Published by the Royal Society of Chemistry

Open Access Article. Published on 03 enero 2022. Downloaded on 20/12/2025 09:30:08 a. m..
This article is licensed under a Creative Commons Attribution-NonCommercial 3.0 Unported Licence.

The quantized circularly polarized standing wave can be written as

$$\mathbf{E}_{c,+} = 2i\mathcal{E}\cos(\mathbf{k}\cdot\mathbf{r})\left[\mathbf{e}_+ a\, e^{-i\omega_c t} - \mathbf{e}_- a^\dagger\, e^{i\omega_c t}\right] \quad (3)$$

where $\mathbf{e}_\pm = \frac{1}{\sqrt{2}}(\mathbf{e}_y \pm i\mathbf{e}_z)$ are the polarization vectors, a and $a^\dagger$ are creation and annihilation operator of cavity mode respectively and $\mathcal{E} = \sqrt{\frac{\hbar\omega_c}{2V\varepsilon_0}}$ is the vacuum electric field amplitude where V is the cavity volume and ε_0 is vacuum permittivity. $H_c = \hbar\omega_c\left(a^\dagger a + \frac{1}{2}\right)$ is the cavity Hamiltonian. The molecule/cavity interaction Hamiltonian is

$$H_I = 2\mathcal{E}i[a\mathbf{e}_+ - a^\dagger\mathbf{e}_-]\cdot\sum_{n=1}^{N}\boldsymbol{\mu}^{(n)} \quad (4)$$

where $\boldsymbol{\mu} = \boldsymbol{\mu}^+ + \boldsymbol{\mu}^-$ is electric dipole of single molecule, $\boldsymbol{\mu}^\pm$ are raising and lowering electric dipole operators which excite and deexcite the molecule and N is the number of molecules. Defining collective ground state $|G\rangle = |g_1 g_2 \ldots g_N\rangle$ and the totally symmetric collective excited states

$$|M_j\rangle = \frac{1}{\sqrt{N}}\sum_n |g_1 \ldots g_{n-1} m_j^{(n)} g_{n+1} \ldots g_N\rangle \quad (5)$$

the cavity–molecule interaction can be recast in the form

$$H_I = 2gi\sum_j\left[(a\mathbf{e}_+ - a^\dagger\mathbf{e}_-)\cdot\left(\boldsymbol{\mu}_{g,m_j}|G\rangle\langle M_j| + \boldsymbol{\mu}_{m_j,g}|M_j\rangle\langle G|\right)\right] \quad (6)$$

where $g = \sqrt{N}\mathcal{E}$ is the coupling strength. For a plane with area A, $N = nA$, where n is the number of molecules per unit area. Thus the coupling strength $g = \sqrt{\frac{n\hbar\omega_c}{2L\varepsilon_0}}$ where L is the distance between the cavity mirrors. The terms containing $a\boldsymbol{\mu}^+$ and $a^\dagger\boldsymbol{\mu}^-$ in eqn (6) represent the polariton interaction, while $a\boldsymbol{\mu}^-$ and $a^\dagger\boldsymbol{\mu}^+$ are counter-rotating terms.

The total Hamiltonian is $H = H_{mol}\otimes I_c + H_c\otimes I_{mol} + H_I$. The joint light-matter states $|M_j, n\rangle = |M_j\rangle \otimes |n\rangle$ are given by direct products of molecular and cavity-photon number states. The polariton states denoted $|P_\alpha\rangle$ ($\alpha = 0, 1, 2, 3\ldots$) are obtained by diagonalizing this Hamiltonian in the joint molecule–cavity space, where α runs over polariton states.

We use a left-circularly polarized pulse

$$\mathscr{E}_{left}(t) = E_0\left[\mathbf{e}_y\cos(\Omega(t-\tau)) - \mathbf{e}_z\sin(\Omega(t-\tau))\right]\exp\left[-\frac{(t-\tau)^2}{2\sigma^2}\right] \quad (7)$$

and a linearly polarized pulse $\mathscr{E}_{linear}(t) = E_0\mathbf{e}_y\cos(\Omega(t-\tau))\exp\left[-\frac{(t-\tau)^2}{2\sigma^2}\right]$ to excite the molecule. We assume that the external laser fields couple directly to the molecules. We used the pulse amplitude $E_0 = 5.14\times10^7$ V cm^{-1} (intensity $I = 3.51\times10^{12}$ W cm^{-2}) and Ω is resonant with $|P_0\rangle$ to $|P_1\rangle$ transition energy. σ is 0.072 6 fs (or 3.0 a.u.) ($\frac{1}{\sigma} = \frac{1}{3}E_H$ in energy domain) so that the pulse bandwidth selectively excites only the $|P_1\rangle$, $|P_2\rangle$ polariton states. Since the ground state energy in the chiral cavity is not very different from the vacuum (see Fig. 3), the ionization potential (IP) in the cavity, which can be approximated by the energy difference of the ground state of cation and neutral molecule, will be essentially the same as in the vacuum. With IP = 6.9 eV,[33] the ionization rate is estimated with the tunneling ionization model[53,54] as 9.7×10^7 s^{-1}, which is negligible. Thus, the ionization process is neglected. The polariton dynamics was calculated by solving the time dependent Schrödinger equation

$$i\hbar\frac{\partial|\psi(t)\rangle}{\partial t} = [H - \boldsymbol{\mu}\cdot\mathbf{E}(t)]|\psi(t)\rangle \quad (8)$$

where ψ is the state for the entire polariton system, and the Hamiltonian H is represented in the polariton eigen states. The evolution was calculated between $t_0 = -9.0$ fs and $t_f = 27$ fs and the pulse is centered at $t = 0.0$ fs. Since the fastest motion in the system is C–H stretching which has 11 fs period, the nuclear motions are frozen during the evolution.

The polariton induced ring currents are monitored by the CD spectroscopy. The signal measured at frequency ω after the pump pulse is over is derived using time-dependent perturbation theory[46]

$$S_{CD}(\omega) = \frac{2}{\hbar^2}\mathrm{Re}\sum_{e,e',e''}|A_{pr}(\omega)|^2\rho_{ee'}\left[\frac{\mathbf{j}_{e'e''}(\mathbf{k}_s)\times\mathbf{j}^\dagger_{e''e}(-\mathbf{k}_s)}{\omega-\omega_{e''e'}+i\Gamma} - \frac{\mathbf{j}_{e''e}(\mathbf{k}_s)\times\mathbf{j}^\dagger_{e''e'}(-\mathbf{k}_s)}{-\omega-\omega_{ee''}+i\Gamma}\right]\cdot\mathbf{e}_x \quad (9)$$

where e, e', e'' run over the polariton states. $\rho_{ee'} = \langle e|\psi\rangle\langle\psi|e'\rangle$ is the polariton density matrix at t_f. $\mathbf{k}_s = \frac{\omega}{c}\mathbf{e}_x$ and $A_{pr}(\omega)$ are the wave vector and the vector potential envelope of the probe pulse, respectively. $\mathbf{j}_{e'e''}(\mathbf{k}_s) = \int d\mathbf{r}\mathbf{j}_{e'e''}(\mathbf{r})\, e^{-i\mathbf{k}_s\cdot\mathbf{r}}$ is the Fourier transformed transition current density. $\hbar\omega_{e''e'} = E_{e''} - E_{e'}$ is the energy difference between two states. The ladder diagram representing eqn (9) is shown in Fig. 2. All CD spectra were simulated for $N = 1$ to exclude two-exciton states from different molecules in the double excitation manifold.

For MCD, we apply $B = 8$ T magnetic field along the x axis and simulate the CD spectrum with linear response TDDFT[55–57]

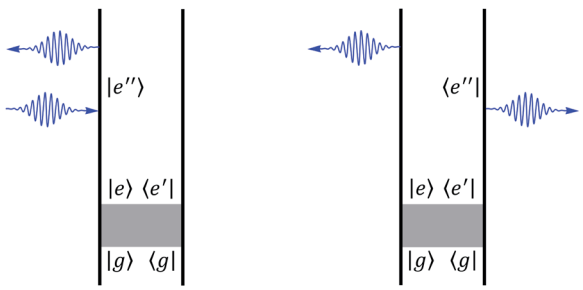

Fig. 2 Ladder diagrams of the circular dichroism signal. The left and right diagrams correspond to first and second term in eqn (9) respectively. The gray zone is the pump pulse with either a linearly polarized pulse or circularly polarized pulse. After the pump pulse, the polariton is excited and described by density matrix $\rho_{ee'}$. A CD measurement is done with circularly polarized pump pulse at a later time.

Open Access Article. Published on 03 enero 2022. Downloaded on 20/12/2025 09:30:08 a. m..
This article is licensed under a Creative Commons Attribution-NonCommercial 3.0 Unported Licence.

using the same density functional and basis set used in TDA calculations.

Results and discussion

Ring current in the chiral polariton states

To study the chiral polaritons of Mg-porphyrin in a chiral cavity, we first identify the polariton states that carry a ring current. We set the detuning $\delta = 0$ eV and the coupling strength $g = 1.028 \times 10^{-1}$ V Å^{-1} (0.002 a.u.) where $|g\boldsymbol{\mu}_{g,m+}| = 1.8 \times 10^{-3}$ eV. With strong light-matter coupling, the ring-current-carrying bare molecular excited state $|M_+\rangle = \frac{1}{\sqrt{2}}(-|M_2\rangle + i|M_1\rangle)$ (see eqn (1) and (5)) together with higher-lying excited states, hybridize with the cavity photon state $|1\rangle$ to form two polariton states $|P_1\rangle$ and $|P_2\rangle$ while the degenerate state $|M_-\rangle = \frac{1}{\sqrt{2}}(-|M_2\rangle - i|M_1\rangle)$ remains intact, as shown in Fig. 3. The higher-lying excited states play an important role in the formation of polariton states because their large detuning is compensated by the stronger transition dipole moment. Similar effects were observed for a transition metal complex.[30] Had we retained only the resonant $|M_\pm\rangle$ states, the polariton states $|P_{1/2}\rangle$ would be an equal mixture of states $|M_+, 0\rangle$ and $|G, 1\rangle$ as in the Jaynes–Cummings model. However, $|P_2\rangle$ is primarily $|M_+, 0\rangle$ whereas $|P_1\rangle$ is primarily $|G, 1\rangle$. The $|P_1\rangle$ and $|P_2\rangle$ states with Rabi splitting 27 meV carry an overall counterclockwise ring current as displayed in Fig. 5 with a spatial profile similar to the molecular ring current induced by a circularly polarized pump.[33] The currents inside and outside the ring have the same direction.

In a chiral cavity, the molecule–cavity interaction has the contribution of $\boldsymbol{\mu}_{Mj,G}\langle 1|a^\dagger|0\rangle$ in eqn (6). Through the counter-rotating term coupling $(a\boldsymbol{\mu}^- - a^\dagger\boldsymbol{\mu}^+)$ between $|G, 0\rangle$ and $|M_j, 1\rangle$, the chiral cavity perturbs and creates a ring current in the polariton ground state $|P_0\rangle$ as shown in Fig. 4. Even the ground state energy does not change much at $g = 1.028 \times 10^{-1}$ V Å^{-1} in Fig. 3, the existence of ground state current shows the effect the counter-rotating term before even reaching the ultrastrong coupling regime, which is a direct evidence of time reversal symmetry breaking. The ground state current has more interesting features than the polariton excited state current. Apart from the overall counterclockwise current around the porphyrin, each pyrrole ring has its local ring current. The current around the Mg cation inside the porphyrin is in the opposite direction than the outside current.

Integrating the current density over the half plane shows that the current in the polariton ground state (1.6×10^{-8} A) is weaker than $|P_1\rangle$ (7.9×10^{-6} A) and $|P_2\rangle$ (7.4×10^{-5} A). The $|P_2\rangle$ current is stronger since it has more contribution from $|M_+, 0\rangle$ than $|P_1\rangle$. The induced magnetic field on the Mg is 7.7×10^{-6}

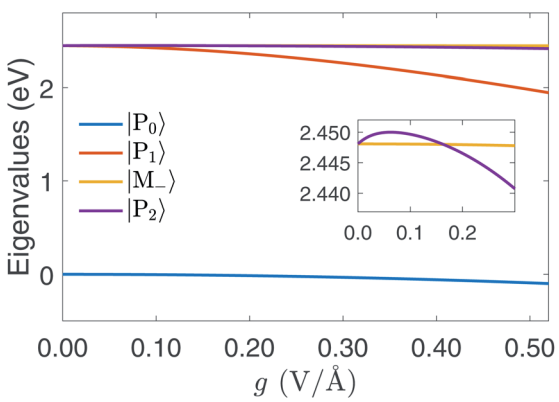

Fig. 3 Polariton energy variation with g for detuning $\delta = 0$. The splitting of $|P_1\rangle$ and $|P_2\rangle$ increase with g. The energy of $|P_2\rangle$ is lower than $|M_-\rangle$ for $g > 0.16$ V Å^{-1}.

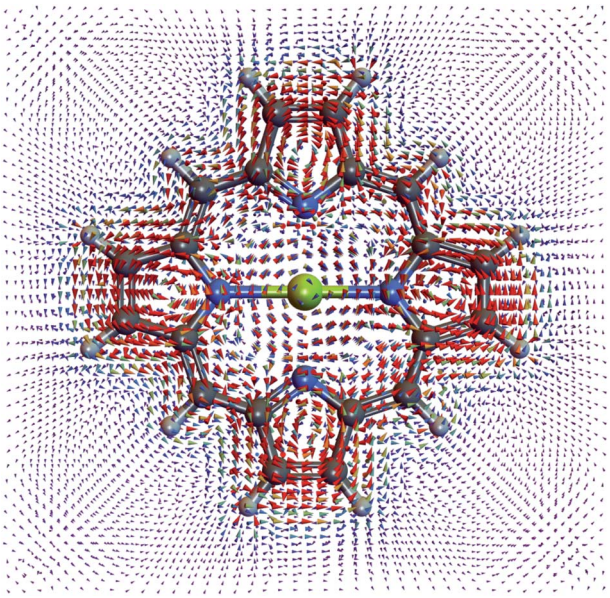

Fig. 4 Current density profile of the polariton ground state.

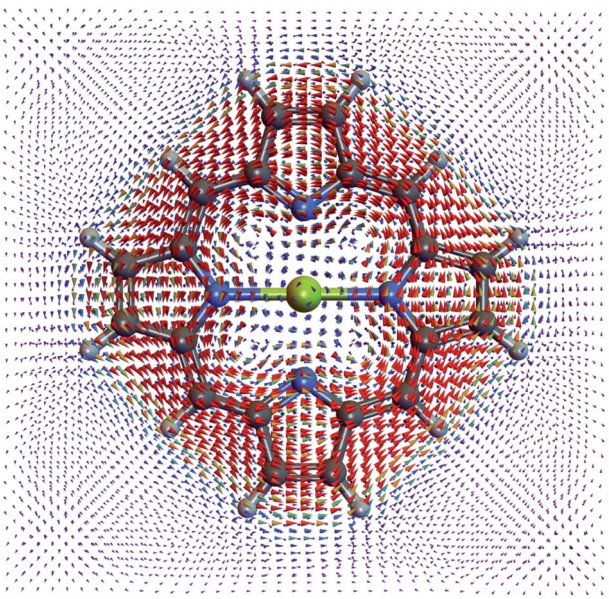

Fig. 5 Current density profile of the $|P_1\rangle$ polariton state. The ring current of $|P_2\rangle$ is similar but stronger.

© 2022 The Author(s). Published by the Royal Society of Chemistry

Open Access Article. Published on 03 enero 2022. Downloaded on 20/12/2025 09:30:08 a. m..
This article is licensed under a Creative Commons Attribution-NonCommercial 3.0 Unported Licence.

T for polariton ground state, 1.6×10^{-2} T for $|P_1\rangle$, and 1.5×10^{-1} T for $|P_2\rangle$.

Polariton ring-currents created by a circularly polarized pump pulse

The excited state polariton ring current is created by an external pump pulse. The time evolution of ground state and excited state populations for circularly polarized pulse eqn (7) is depicted in the top panel of Fig. 6. The applied pulse brings the ground state to the polariton state $|P_1\rangle$. $|P_2\rangle$ has a very small population since the oscillator strength from $|P_0\rangle$ to $|P_2\rangle$ is much weaker. The unperturbed excited state $|M_-\rangle$ is not populated due to the selection rule. To probe the ring current, we have simulated the CD of the polariton states in UV-visible regime following a circularly polarized pulse shown in Fig. 8 top panel.

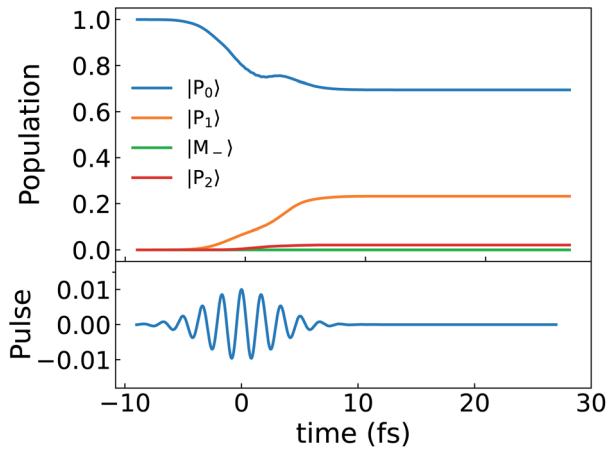

Fig. 6 Top: population dynamics (eqn (8)) of the polariton states for a Mg-porphyrin in the chiral cavity excited by a circularly polarized pulse. Bottom: y component of the electric field of the pump pulse.

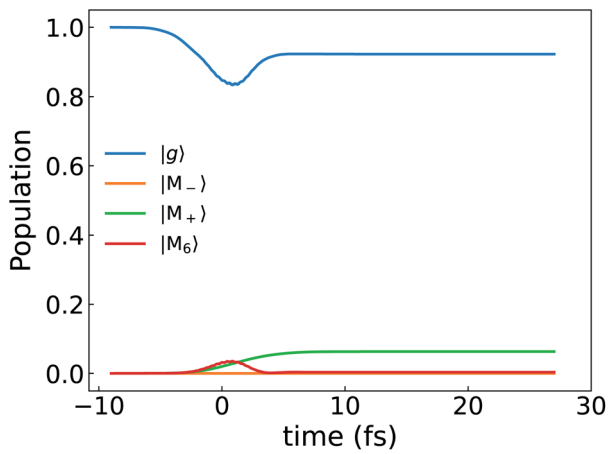

Fig. 7 Population dynamics of the Mg-porphyrin molecule excited by a circularly polarized pulse same as Fig. 6. The molecular excited state 6 is slightly populated as well.

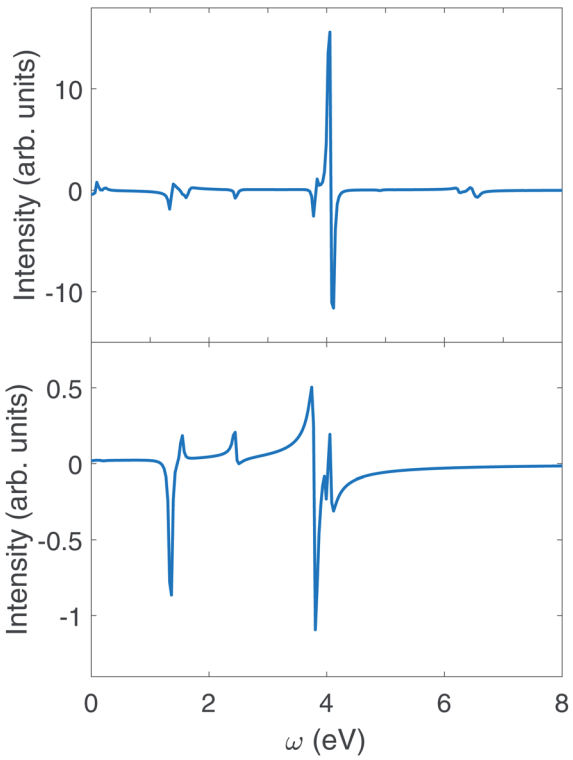

Fig. 8 CD signals eqn (9) of polariton in the chiral cavity with $\delta = 0$, $g = 1.028 \times 10^{-1}$ V Å^{-1} (or 0.002 a.u.) (top), and no cavity (bottom). The CD measurement follows a circularly polarized pump pulse in both polariton and bare molecule.

For comparison, we present the same quantities for the bare (no cavity) Mg-porphyrin molecule in Fig. 7 and 8 bottom panel. The right circularly polarized light selectively excites the state $|M_+\rangle$, which carries a ring current.

We first observe an order of magnitude enhanced polariton CD signal around 4.0 eV. In the CD signal without cavity, the peaks between 3.7 eV and 4.1 eV have those contributions: At 3.795 9 eV, the excitation is from $|G\rangle$ to $|M_3\rangle$ has intensity $\rho_{M_+,G}\mathbf{j}_{G,M_3} \times \mathbf{j}^{\dagger}_{M_3,M_+}$, and transition from $|M_3\rangle$ to $|G\rangle$ with intensity $\rho_{G,M_+}\mathbf{j}_{M_3,G} \times \mathbf{j}^{\dagger}_{M_3,M_+}$. At 4.060 1 eV, the transition from $|M_9\rangle$ to $|G\rangle$ with intensity $\rho_{G,M_+}\mathbf{j}_{M_9,G} \times \mathbf{j}^{\dagger}_{M_9,M_+}$. However, in polariton CD, the 3.7 to 4.1 eV regime is dominated by a group of much stronger peaks. We can assign the contributions of various polariton states by examining the numerator in the CD expression eqn (9). The strongest 4.1 eV peaks correspond to two pairs of transitions: (1) excitation from the ground state $|P_0\rangle$ to the polariton states $|P_{10}\rangle$, $|P_{11}\rangle$, which mainly consist of $-i|M_8, 0\rangle + |M_9, 0\rangle$ and $i|M_8, 0\rangle + |M_9, 0\rangle$ respectively; (2) excitation from lower polariton state $|P_1\rangle$ (mainly consist of $|G, 1\rangle$) to polariton state $|P_{21}\rangle$ and $|P_{23}\rangle$, which primarily consist of $i|M_8, 1\rangle - |M_9, 1\rangle$ and $-i|M_8, 1\rangle - |M_9, 1\rangle$ respectively. Note that the degenerate molecular states $|M_8\rangle$ and $|M_9\rangle$ with E_u irreducible representation have electric dipole along y and $-z$ respectively (Table S1†). In order to explain the CD signal enhancement, we define degenerate molecular states $|M^{II}_{\pm}\rangle = \frac{1}{\sqrt{2}}(\pm i|M_8\rangle - |M_9\rangle)$. Their CD signal strengths of

Open Access Article. Published on 03 enero 2022. Downloaded on 20/12/2025 09:30:08 a. m..
This article is licensed under a Creative Commons Attribution-NonCommercial 3.0 Unported Licence.

molecular systems are determined by $\mathbf{j}_{G,M_+^{II}} \times \mathbf{j}_{M_+^{II},G}$ and $\mathbf{j}_{G,M_-^{II}} \times \mathbf{j}_{M_-^{II},G}$ (eqn (9)), which have the same magnitude but an opposite sign. Since the molecular states $|M_+^{II}\rangle$ and $|M_-^{II}\rangle$ are degenerate, their CD signals cancel out. For the polariton states $|P_{10}\rangle$ and $|P_{11}\rangle$, the CD signal strength $\mathbf{j}_{P_0,P_{10}} \times \mathbf{j}_{P_{10}P_0}$ and $\mathbf{j}_{P_0P_{11}} \times \mathbf{j}_{P_{11}P_0}$ have a similar magnitude but an opposite sign. Due to their coupling with the chiral cavity, states $|P_{10}\rangle$ and $|P_{11}\rangle$ are non degenerate. We thus see a strong positive peak and negative peak next to each other in the polariton spectrum around 4.1 eV. The cause of the strong CD signal from $|P_1\rangle$ to the polariton states $|P_{21}\rangle$ and $|P_{23}\rangle$ is similar. Since $|P_1\rangle$ carries a polariton ring current, the 4.1 eV peak can be viewed as partially ring current CD signal and partially ground state excitation signal.

To further confirm that the enhancement of CD is caused by the chiral cavity, we place the molecule in a non-chiral cavity with a linearly polarized standing wave $\mathbf{E}_{st} = 2i\mathcal{E}\cos(\mathbf{k}\cdot\mathbf{r})[\mathbf{e}_{yz}a\,e^{-i\omega_c t} - \mathbf{e}_{yz}a^{\dagger}\,e^{i\omega_c t}]$, where the polarization vector is $\mathbf{e}_{yz} = \frac{1}{\sqrt{2}}(\mathbf{e}_y + \mathbf{e}_z)$. The polarization vectors $\mathbf{e}_+$, $\mathbf{e}_-$ in the molecule–cavity interaction Hamiltonian (eqn (6)) are replaced by the linearly polarization vector $\mathbf{e}_{yz}$. The resulting CD signal shown in Fig. 9 has a similar magnitude to that of the bare molecule. The enhancement of CD signal (top panel of Fig. 8) is thus due to the chiral modes.

The weaker peaks in the polariton CD signal in the top panel of Fig. 8 also contain signatures of polariton states. The 6.495 3 eV peak in the polariton CD is mainly the excitation from $|P_0\rangle$ to $|P_{21}\rangle$ (mostly $i|M_8, 1\rangle - |M_9, 1\rangle$), with intensity $\rho_{P_1,P_0}\mathbf{j}_{P_0,P_{21}} \times \mathbf{j}^{\dagger}_{P_{21},P_1}$. Such peaks do not exist in the bare molecule CD signal shown in the lower panel of Fig. 8.

There are also some noticeable differences between the bare molecule and the polaritons in some groups of peaks. Without cavity, the 2.448 1 eV peak corresponds to the transition from the ground state to $|M_+\rangle$ with intensity $\rho_{G,M_7}\mathbf{j}_{M_+,G} \times \mathbf{j}^{\dagger}_{M_+,M_7}$. For polariton CD, the peak at 2.451 9 eV is the excitation from ground state $|P_0\rangle$ to $|M_-\rangle$ with intensity $\rho_{P_0,P_0}\mathbf{j}_{P_0,M_-} \times \mathbf{j}^{\dagger}_{M_-,P_0}$. The peaks at 2.453 4 eV and 2.426 3 eV represent excitations from ground state to upper and lower polariton states, with intensity $\rho_{P_0,P_0}\mathbf{j}_{P_0,P_2} \times \mathbf{j}^{\dagger}_{P_2,P_0}$ and $\rho_{P_0,P_0}\mathbf{j}_{P_0,P_1} \times \mathbf{j}^{\dagger}_{P_1,P_0}$ respectively. Such excitations are not present in the bare molecule, due to the cancellation of signal of the degenerate states with E_u irreducible representation (see Table S1†).

The intensity of the group of peaks around 1.4 eV is similar for the bare molecule and polaritons. In the bare molecule, the negative 1.347 8 eV peak corresponds to the excitation from $|M_+\rangle$ to excited state $|M_3\rangle$ and its strength is determined by $\rho_{M_+,M_+}\mathbf{j}_{M_+,M_3} \times \mathbf{j}^{\dagger}_{M_3,M_+}$ (first term in eqn (9)). The positive 1.536 3 eV peak arises from the transition from $|M_+\rangle$ to $|M_7\rangle$, whose intensity is determined by $\rho_{M_+,M_+}\mathbf{j}_{M_+,M_7} \times \mathbf{j}^{\dagger}_{M_7,M_+}$. A similar excitation can be found in the polariton CD spectrum at 1.33 eV. The negative peak has two contributions: (1) the excitation from $|P_2\rangle$ to $|P_5\rangle$ (mostly $|M_3, 0\rangle$) with intensity $\rho_{P_0,P_2}\mathbf{j}_{P_2,P_5} \times \mathbf{j}^{\dagger}_{P_5,P_0}$; (2) the transition from $|P_5\rangle$ to $|P_2\rangle$ with intensity $\rho_{P_2,P_1}\mathbf{j}_{P_5,P_2} \times \mathbf{j}^{\dagger}_{P_5,P_1}$. The positive peak has two contributions: (1) $|P_5\rangle$ to $|P_1\rangle$, with intensity $\rho_{P_1,P_0}\mathbf{j}_{P_5,P_1} \times \mathbf{j}^{\dagger}_{P_5,P_0}$; (2) transition from $|P_5\rangle$ to $|P_1\rangle$, with intensity $\rho_{P_1,P_2}\mathbf{j}_{P_5,P_1} \times \mathbf{j}^{\dagger}_{P_5,P_2}$.

Polariton ring currents created by a linearly polarized light

Unlike the bare molecules, the polariton ring currents can be induced by a linearly polarized light. The population dynamics is shown in Fig. 10. Following the pulse, the lower polariton state $|P_1\rangle$ population increases significantly, while the unperturbed state $|M_-\rangle$ only slightly increases since the transition dipole of ground state and lower polariton state $\boldsymbol{\mu}_{P0,P1}$ is much larger than that to the unperturbed state $\boldsymbol{\mu}_{P0,M-}$. The lower polariton state $|P_1\rangle$ is dominated by $|G, 1\rangle$. Since the transition dipoles between ground state and higher excited states (*e.g.*, excited state 4, 5, 8, 9 in Table S1†) are about 10 times higher than $\boldsymbol{\mu}_{G,M+}$ and $\boldsymbol{\mu}_{G,M-}$, the lower polariton state $|P_1\rangle$ is mixed with these higher excited states through resonant interaction of the molecule–cavity coupling, for example $\langle G, 1|\boldsymbol{\mu}a^{\dagger}|M_9, 0\rangle$. The mixing of higher energy excited states with large detunings in the polariton states does not require counter-rotating terms, although there are extra contributions from them, for example, $\langle M_+, 0|\boldsymbol{\mu}a|M_9, 1\rangle$. The transition dipole $\boldsymbol{\mu}_{G,P1}$ is thus much higher than $\boldsymbol{\mu}_{G,M-}$, which causes a population difference

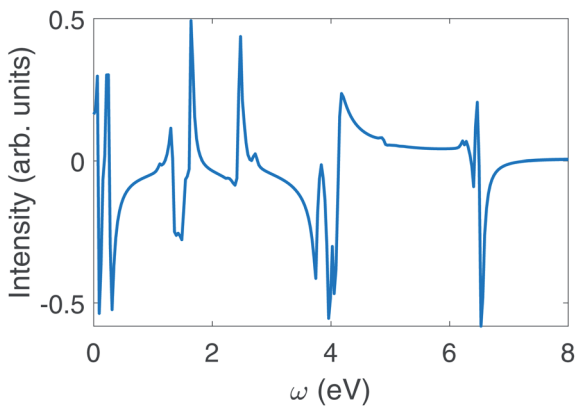

Fig. 9 CD signal eqn (6) of polariton with $\delta = 0$, $g = 0.002$ for Mg-porphyrin molecule in the linearly polarized cavity excited by circularly polarized pulse.

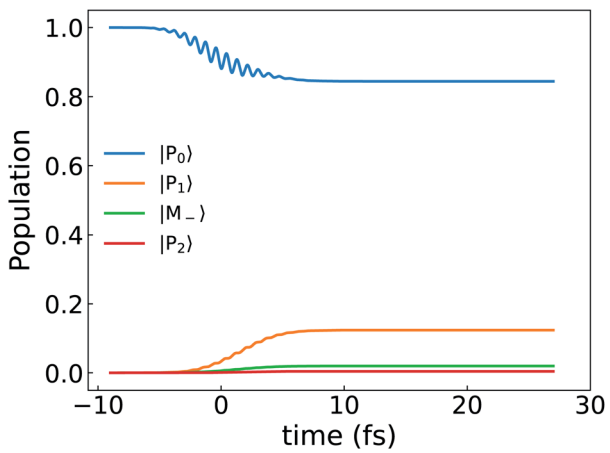

Fig. 10 Population dynamics of polariton states created by a linearly polarized light pulse with $\delta = 0$, $g = 1.028 \times 10^{-1}$ V Å^{-1}.

© 2022 The Author(s). Published by the Royal Society of Chemistry

Open Access Article. Published on 03 enero 2022. Downloaded on 20/12/2025 09:30:08 a. m..
This article is licensed under a Creative Commons Attribution-NonCommercial 3.0 Unported Licence.

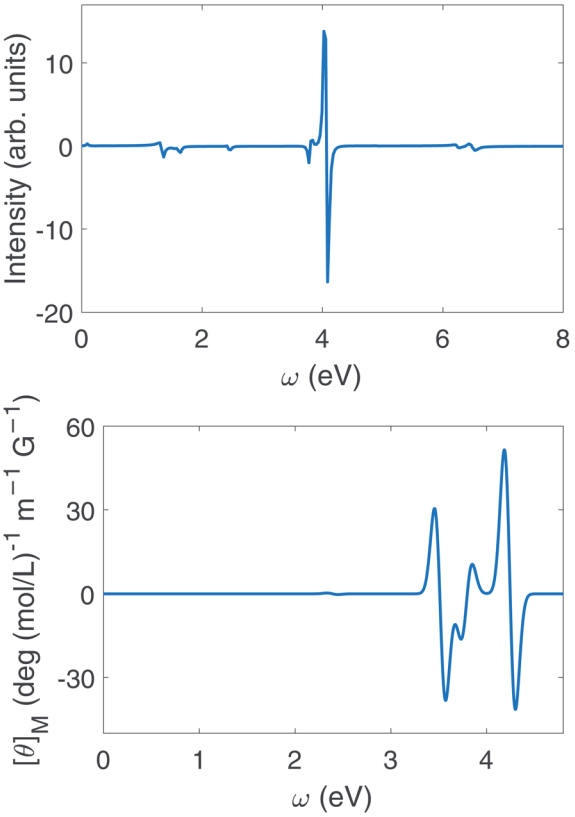

Fig. 11 Upper panel: circular dichroism spectrum eqn (9) of polaritons with $\delta = 0$, $g = 1.028 \times 10^{-1}$ V Å^{-1} excited by linearly polarized pulse. Lower panel: magnetic circular dichroism of Mg-porphyrin molecule in the magnetic field of 8 T (or 3.403 5 $\times 10^{-5}$ a.u.).

following the linear polarized pulse, thus creating a ring current. The CD spectrum of polariton excited by linearly polarized light is shown in the upper panel of Fig. 11. Enhancement of the CD spectrum in both linearly polarized light excitation (upper panel of Fig. 11) and in circularly polarized light excitation (upper panel of Fig. 8) originates from the excitations from $|P_0\rangle$ and $|P_1\rangle$ to higher excited states $|P_{10}\rangle$, $|P_{11}\rangle$, $|P_{21}\rangle$, $|P_{23}\rangle$. The degeneracy of $|P_{10}\rangle$ and $|P_{11}\rangle$ and of $|P_{21}\rangle$ and $|P_{23}\rangle$ are lifted by the chiral cavity mode.

Signatures of detuning and coupling strength

The polariton state energies for zero detuning δ and different coupling strengths g are depicted in Fig. 3. In the weak coupling region ($g < 1.6 \times 10^{-1}$ V Å^{-1}), state $|M_-\rangle$ is higher than $|P_1\rangle$ and lower than $|P_2\rangle$. For $g > 1.6 \times 10^{-1}$ V Å^{-1}, $|M_-\rangle$ is higher than $|P_2\rangle$.

In Fig. 12, we vary the coupling g from 2.056×10^{-1} V Å^{-1} to 5.142×10^{-1} V Å^{-1} (or from 0.004 to 0.010 a.u.) holding the detuning $\delta = 0$, and use a circularly polarized light pulse to initiate the dynamics.

Comparing Fig. 6 with the left panel of Fig. 12, we find that the population of the polariton state $|P_{12}\rangle$ dominated by $|G, 2\rangle$ increases with coupling strength. As g is increased to 5.142 V Å^{-1}, the population of $|P_{12}\rangle$ (dominated by $|G, 2\rangle$) is much higher than the lower polariton state $|P_1\rangle$ (dominated by $|G, 1\rangle$) after the pulse.

The variation of the polariton state energies with detuning is depicted in Fig. 13 for a fixed coupling strength $g = 1.028 \times 10^{-1}$ V Å^{-1}. The population evolution and the CD spectra are displayed in Fig. 14. For $\delta < 0$, the lower polariton state $|P_1\rangle$ is dominated by $|M_+, 0\rangle$ while the upper polariton $|P_2\rangle$ is

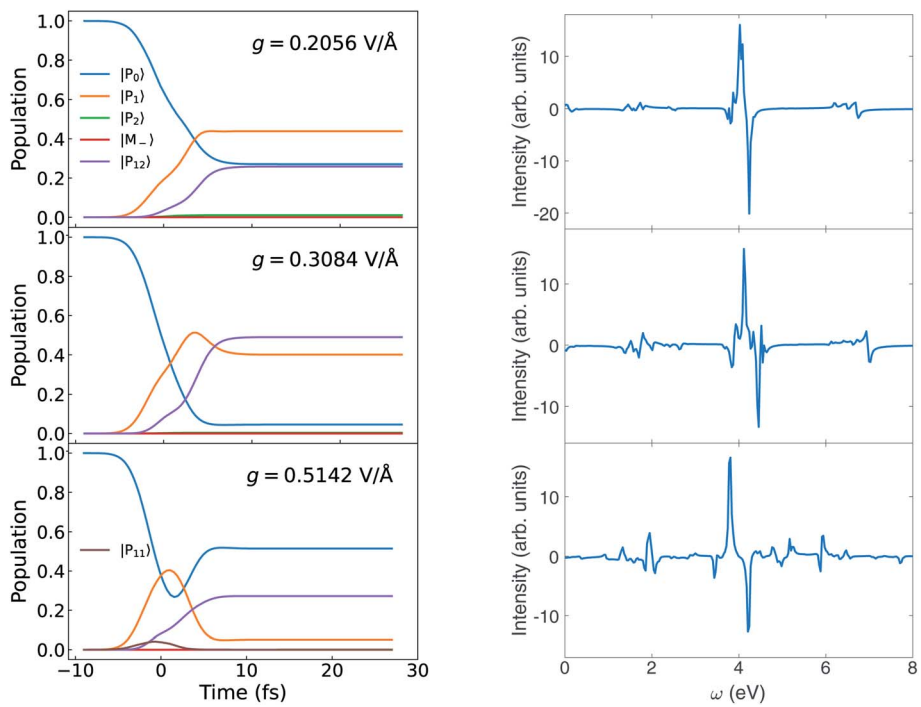

Fig. 12 Left: Population dynamics for different g at $\delta = 0$. Right: Circular dichroism signal eqn (9) for different g at $\delta = 0$.

Open Access Article. Published on 03 enero 2022. Downloaded on 20/12/2025 09:30:08 a. m..
This article is licensed under a Creative Commons Attribution-NonCommercial 3.0 Unported Licence.

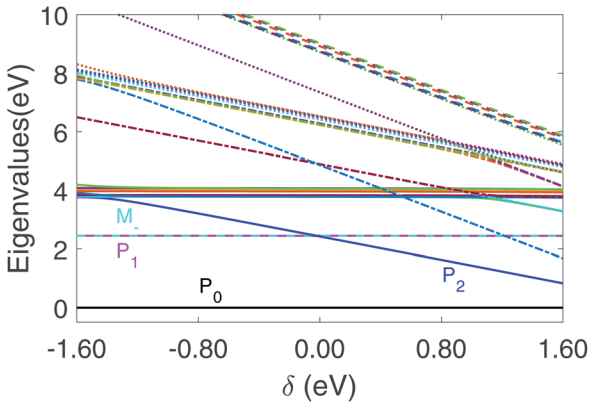

Fig. 13 Polariton energy variation with detuning for coupling strength $g = 1.028 \times 10^{-1}$ V Å^{-1}. We mark $|P_0\rangle$, $|P_1\rangle$, $|P_2\rangle$, $|M_-\rangle$ with color. The legend of other polariton states are given in Fig. S1 in ESI.†

dominated by $|G, 1\rangle$. For $\delta > 0$, $|P_1\rangle$ is dominated by $|G, 1\rangle$ and $|P_2\rangle$ is dominated by $|M_+, 0\rangle$. Since the polariton state dominated by $|G, 1\rangle$ can mix with higher excited states through $\boldsymbol{\mu}_{G,Mj}$, and increase the polariton transition dipole, these states can be highly populated by the circularly polarized pulse. This explains why the $|P_1\rangle$ population increases for $\delta < 0$, while $|P_2\rangle$ increase for $\delta > 0$. A similar trend can be found in Fig. 15 for the coupling strength $g = 3.084 \times 10^{-1}$ V Å^{-1} (or 0.006 a.u.). Due to the larger coupling strength g in Fig. 15, the population has some two photon mode mixed in compared with Fig. 14.

Since the ring current in the polariton states dominated by $|M_+, 0\rangle$ is strong, the cavity detuning δ can be adjusted to promote the polariton state dominated by $|M_+, 0\rangle$ as in Fig. 14 and 15.

Comparison of polariton CD with MCD signals

It is instructive to compare the polariton CD signal with the bare molecule MCD, since both magnetic field and chiral optical

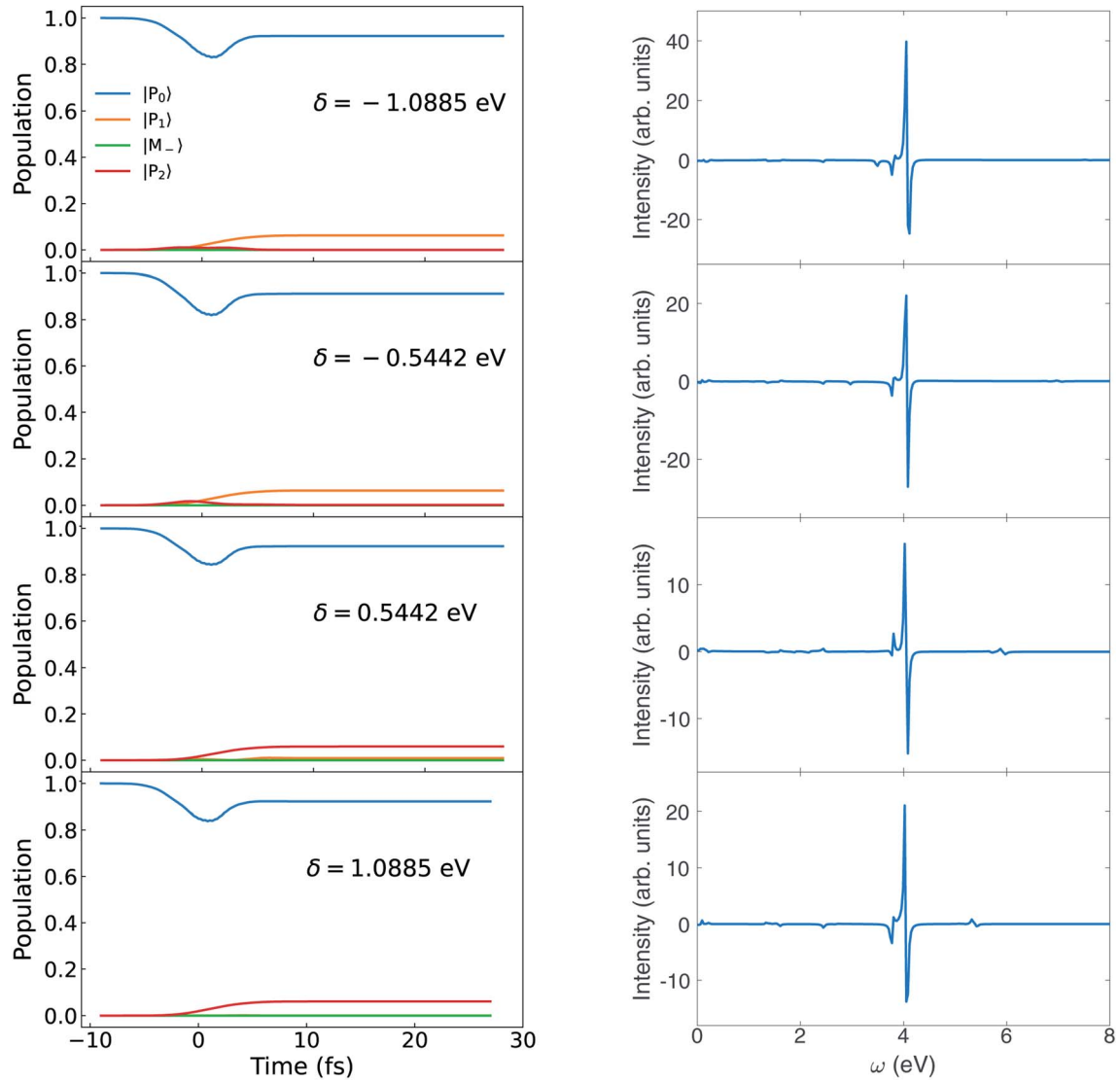

Fig. 14 Left: Population dynamics for different δ at $g = 0.102\,8$ V Å^{-1}. Right: Circular dichroism signal eqn (9) for different δ at $g = 0.102\,8$ V Å^{-1}.

© 2022 The Author(s). Published by the Royal Society of Chemistry

Open Access Article. Published on 03 enero 2022. Downloaded on 20/12/2025 09:30:08 a. m..
This article is licensed under a Creative Commons Attribution-NonCommercial 3.0 Unported Licence.

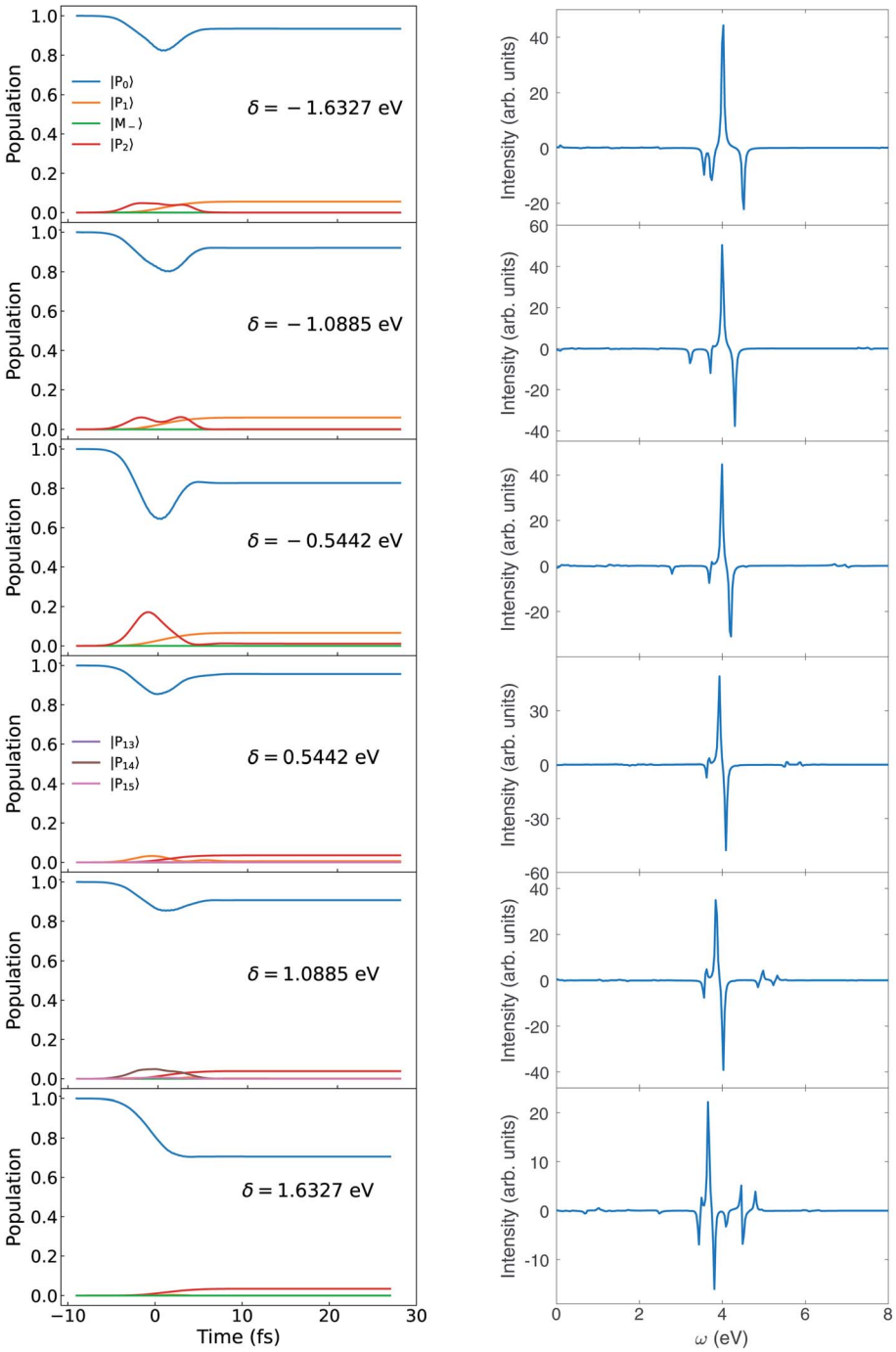

Fig. 15 Left: Population dynamics for different δ at $g = 0.308$ 4 V Å^{-1}. Right: CD spectra eqn (9) for different δ at $g = 0.308$ 4 V Å^{-1}.

cavities lift the excited state degeneracy. The excited states in the presence of magnetic fields are listed in table S2† in ESI.† Since MCD is simulated at the TDDFT level while chiral polaritons use the TDA, there are a small difference in energy. The peaks involving excited states of E_u irreducible representation can be assigned by comparing the upper and lower panel of Fig. 11. The strongest pair of peaks around 4.2 eV in MCD signal is the excitation from ground state to states 12, 13. While the strongest peaks at 4 eV in CD signal of Mg-porphyrin in chiral cavity is caused by the excitation from ground state to states $|P_{10}\rangle$, $|P_{11}\rangle$ which are dominated by $|M_8, 0\rangle$, $|M_9, 0\rangle$. By analyzing the molecular orbital contribution, states 12, 13 in TDDFT are equivalent to states 8, 9 in TDA. Thus the strongest peak of the molecule in the chiral cavity and in the magnetic field have a similar origin, *i.e.*, breaking of degeneracy in excited states with E_u irreducible representation. The degeneracy is broken in the magnetic field by orbital Zeeman effect, since the angular momentum along the C_4 rotation axis of the molecule is opposite in the degenerate E_u excited states. In the chiral cavity, the degeneracy is broken since the cavity mode is only coupled

Open Access Article. Published on 03 enero 2022. Downloaded on 20/12/2025 09:30:08 a. m..
This article is licensed under a Creative Commons Attribution-NonCommercial 3.0 Unported Licence.

with one excited state in that pair of E_u degenerate states and leaving the other state unperturbed. This results in a pair of peaks with opposite sign.

Similarly, a pair of weak MCD peaks at 2.38 eV originate from excited states 1, 2, while the peaks in polariton CD around 2.4 eV are from $|P_1\rangle$, $|P_2\rangle$ and $|M_-\rangle$. These are also caused by the degeneracy breaking of states with E_u irreducible representation.

Summary

Chiral cavities open up numerous opportunities to for controlling photophysical properties of molecules. By exploring the effects of a chiral cavity on the ring current in Mg-porphyrin, we showed that the CD signal can be enhanced. We found a ring current in both ground state and polariton excited states made with chiral cavity. A strong polariton ring current can be created in the Mg-porphyrin in a chiral cavity by either a circularly polarized pulse or a linearly polarized light pulse. Due to cavity-induced coupling of the molecular ground state to higher excited state, the excitation from the ground state to the $|P_1\rangle$ polariton state is stronger than to the unperturbed molecular state $|M_-\rangle$. As a result, even a linearly polarized light can selectively excite the polariton state and create a strong ring current.

This can be detected by a circular dichroism measurement after the pump pulse. The chiral cavity breaks the degeneracy of excited states with the E_u irreducible representation in cyclic conjugated molecules, resulting in pairs of peaks with opposite sign, which makes the polaritonic CD signal one order of magnitude stronger than in the bare molecule pumped with circularly polarized pulse. These results clearly demonstrate the utility of chiral cavities to manipulate photochemical processes of molecules. Future extensions of this study include incorporating the vibronic coupling,[58–60] cavity leakage, and many-molecule collective dark states[29] into the model. The chiral cavity-induced time reversal symmetry breaking may also be employed to create topological states.[61]

Data availability

All study data are included in the article and/or ESI.†

Author contributions

S. M. supervised the project. B. G. and S. S. conceived the project. B. G. implemented the code for polaritonic dynamics. S. S. performed the electronic structure calculations, polariton and spectroscopy simulations. All authors contributed to the analysis and interpretation of the results, and wrote the manuscript.

Conflicts of interest

There are no conflicts to declare.

Acknowledgements

The support of the National Science Foundation through Grant No. CHE-1953045 is gratefully acknowledged. S. M. was supported by the U.S. Department of Energy, Office of Science, Office of Basic Energy Sciences under award DE-SC0022134.

References

1 F. Herrera and J. Owrutsky, Molecular Polaritons for Controlling Chemistry with Quantum Optics, *J. Chem. Phys.*, 2020, **152**, 100902.
2 D. Sidler, C. Schäfer, M. Ruggenthaler and A. Rubio, Polaritonic Chemistry: Collective Strong Coupling Implies Strong Local Modification of Chemical Properties, *J. Phys. Chem. Lett.*, 2020, 508–516.
3 T. W. Ebbesen, Hybrid Light–Matter States in a Molecular and Material Science Perspective, *Acc. Chem. Res.*, 2016, **49**, 2403–2412.
4 X. Zhong, T. Chervy, S. Wang, J. George, A. Thomas, J. A. Hutchison, E. Devaux, C. Genet and T. W. Ebbesen, Non-Radiative Energy Transfer Mediated by Hybrid Light-Matter States, *Angew. Chem.*, 2016, **128**, 6310–6314.
5 X. Zhong, T. Chervy, L. Zhang, A. Thomas, J. George, C. Genet, J. A. Hutchison and T. W. Ebbesen, Energy Transfer between Spatially Separated Entangled Molecules, *Angew. Chem., Int. Ed.*, 2017, **56**, 9034–9038.
6 J. George, A. Shalabney, J. A. Hutchison, C. Genet and T. W. Ebbesen, Liquid-Phase Vibrational Strong Coupling, *J. Phys. Chem. Lett.*, 2015, **6**, 1027–1031.
7 A. Shalabney, J. George, J. Hutchison, G. Pupillo, C. Genet and T. W. Ebbesen, Coherent Coupling of Molecular Resonators with a Microcavity Mode, *Nat. Commun.*, 2015, **6**, 5981.
8 F. Benz, M. K. Schmidt, A. Dreismann, R. Chikkaraddy, Y. Zhang, A. Demetriadou, C. Carnegie, H. Ohadi, B. de Nijs, R. Esteban, J. Aizpurua and J. J. Baumberg, Single-Molecule Optomechanics in "Picocavities", *Science*, 2016, **354**, 726–729.
9 A. Thomas, L. Lethuillier-Karl, K. Nagarajan, R. M. A. Vergauwe, J. George, T. Chervy, A. Shalabney, E. Devaux, C. Genet, J. Moran and T. W. Ebbesen, Tilting a Ground-State Reactivity Landscape by Vibrational Strong Coupling, *Science*, 2019, **363**, 615–619.
10 J. A. Hutchison, T. Schwartz, C. Genet, E. Devaux and T. W. Ebbesen, Modifying Chemical Landscapes by Coupling to Vacuum Fields, *Angew. Chem., Int. Ed.*, 2012, **51**, 1592–1596.
11 C. Schäfer, M. Ruggenthaler, H. Appel and A. Rubio, Modification of Excitation and Charge Transfer in Cavity Quantum-Electrodynamical Chemistry, *Proc. Natl. Acad. Sci. U. S. A.*, 2019, **116**, 4883–4892.
12 J. Galego, F. J. Garcia-Vidal and J. Feist, Cavity-Induced Modifications of Molecular Structure in the Strong-Coupling Regime, *Phys. Rev. X*, 2015, **5**, 041022.

© 2022 The Author(s). Published by the Royal Society of Chemistry

Open Access Article. Published on 03 enero 2022. Downloaded on 20/12/2025 09:30:08 a. m..
This article is licensed under a Creative Commons Attribution-NonCommercial 3.0 Unported Licence.

13 J. Flick, N. Rivera and P. Narang, Strong Light-Matter Coupling in Quantum Chemistry and Quantum Photonics, *Nanophotonics*, 2018, **7**, 1479–1501.
14 K. E. Dorfman and S. Mukamel, Multidimensional Photon Correlation Spectroscopy of Cavity Polaritons, *Proc. Natl. Acad. Sci. U. S. A.*, 2018, **115**, 1451–1456.
15 F. Herrera and F. C. Spano, Cavity-Controlled Chemistry in Molecular Ensembles, *Phys. Rev. Lett.*, 2016, **116**, 238301.
16 D. M. Coles, N. Somaschi, P. Michetti, C. Clark, P. G. Lagoudakis, P. G. Savvidis and D. G. Lidzey, Polariton-Mediated Energy Transfer between Organic Dyes in a Strongly Coupled Optical Microcavity, *Nat. Mater.*, 2014, **13**, 712–719.
17 A. Frisk Kockum, A. Miranowicz, S. De Liberato, S. Savasta and F. Nori, Ultrastrong Coupling between Light and Matter, *Nat. Rev. Phys.*, 2019, **1**, 19–40.
18 P. Vasa and C. Lienau, Strong Light–Matter Interaction in Quantum Emitter/Metal Hybrid Nanostructures, *ACS Photonics*, 2018, **5**, 2–23.
19 M. Hertzog, M. Wang, J. Mony and K. Börjesson, Strong Light–Matter Interactions: A New Direction within Chemistry, *Chem. Soc. Rev.*, 2019, **48**, 937–961.
20 J. Flick, M. Ruggenthaler, H. Appel and A. Rubio, Atoms and Molecules in Cavities, from Weak to Strong Coupling in Quantum-Electrodynamics (QED) Chemistry, *Proc. Natl. Acad. Sci. U. S. A.*, 2017, **114**, 3026–3034.
21 T. Schwartz, J. A. Hutchison, J. Léonard, C. Genet, S. Haacke and T. W. Ebbesen, Polariton Dynamics under Strong Light–Molecule Coupling, *ChemPhysChem*, 2013, **14**, 125–131.
22 F. Herrera and F. C. Spano, Dark Vibronic Polaritons and the Spectroscopy of Organic Microcavities, *Phys. Rev. Lett.*, 2017, **118**, 223601.
23 L. A. Martínez-Martínez, M. Du, F. Ribeiro, S. Kéna-Cohen and J. Yuen-Zhou, Polariton-Assisted Singlet Fission in Acene Aggregates, *J. Phys. Chem. Lett.*, 2018, **9**, 1951–1957.
24 D. Sanvitto and S. Kéna-Cohen, The Road towards Polaritonic Devices, *Nat. Mater.*, 2016, **15**, 1061–1073.
25 A. Mandal and P. Huo, Investigating New Reactivities Enabled by Polariton Photochemistry, *J. Phys. Chem. Lett.*, 2019, **10**, 5519–5529.
26 K. Bennett, M. Kowalewski and S. Mukamel, Novel Photochemistry of Molecular Polaritons in Optical Cavities, *Faraday Discuss.*, 2016, **194**, 259–282.
27 B. Gu and S. Mukamel, Manipulating Nonadiabatic Conical Intersection Dynamics by Optical Cavities, *Chem. Sci.*, 2020, **11**, 1290–1298.
28 B. Gu and S. Mukamel, Optical-Cavity Manipulation of Conical Intersections and Singlet Fission in Pentacene Dimers, *J. Phys. Chem. Lett.*, 2021, **12**, 2052–2056.
29 B. Gu and S. Mukamel, Cooperative Conical Intersection Dynamics of Two Pyrazine Molecules in an Optical Cavity, *J. Phys. Chem. Lett.*, 2020, **11**, 5555–5562.
30 B. Gu, S. M. Cavaletto, D. R. Nascimento, M. Khalil, N. Govind and S. Mukamel, Manipulating Valence and Core Electronic Excitations of a Transition-Metal Complex Using UV/Vis and X-Ray Cavities, *Chem. Sci.*, 2021, 8088–8095.
31 H. Hübener, U. De Giovannini, C. Schäfer, J. Andberger, M. Ruggenthaler, J. Faist and A. Rubio, Engineering quantum materials with chiral optical cavities, *Nat. Mater.*, 2021, **20**, 438–442.
32 Z. Nelson, L. Delage-Laurin, M. D. Peeks and T. M. Swager, Large Faraday Rotation in Optical-Quality Phthalocyanine and Porphyrin Thin Films, *J. Am. Chem. Soc.*, 2021, **143**, 7096–7103, PMID: 33905654.
33 I. Barth, J. Manz, Y. Shigeta and K. Yagi, Unidirectional Electronic Ring Current Driven by a Few Cycle Circularly Polarized Laser Pulse: Quantum Model Simulations for Mg- porphyrin, *J. Am. Chem. Soc.*, 2006, **128**, 7043–7049, PMID: 16719485.
34 I. Barth and J. Manz, Periodic Electron Circulation Induced by Circularly Polarized Laser Pulses: Quantum Model Simulations for Mg Porphyrin, *Angew. Chem., Int. Ed.*, 2006, **45**, 2962–2965.
35 I. Barth and J. Manz, Electric Ring Currents in Atomic Orbitals and Magnetic Fields Induced by Short Intense Circularly Polarized π Laser Pulses, *Phys. Rev. A: At., Mol., Opt. Phys.*, 2007, **75**, 012510.
36 J. J. Rodriguez and S. Mukamel, Probing Ring Currents in Mg-Porphyrins by Pump–Probe Spectroscopy, *J. Phys. Chem. A*, 2012, **116**, 11095–11100, PMID:22 881200.
37 P. Lazzeretti, Ring Currents, *Prog. Nucl. Magn. Reson. Spectrosc.*, 2000, **36**, 1–88.
38 J. Jusélius and D. Sundholm, The aromatic character of magnesium porphyrins, *J. Org. Chem.*, 2000, **65**, 5233–5237.
39 E. Steiner and P. W. Fowler, Patterns of Ring Currents in Conjugated Molecules: A Few-Electron Model Based on Orbital Contributions, *J. Phys. Chem. A*, 2001, **105**, 9553–9562.
40 G. Merino, T. Heine and G. Seifert, The Induced Magnetic Field in Cyclic Molecules, *Chem.–Eur. J.*, 2004, **10**, 4367–4371.
41 E. Steiner, A. Soncini and P. W. Fowler, Ring currents in the porphyrins: π shielding, delocalisation pathways and the central cation, *Org. Biomol. Chem.*, 2005, **3**, 4053–4059.
42 T. Heine, C. Corminboeuf and G. Seifert, The Magnetic Shielding Function of Molecules and Pi-Electron Delocalization, *Chem. Rev.*, 2005, **105**, 3889–3910, PMID: 16218570.
43 L. D. Barron, *Molecular light scattering and optical activity*, Cambridge University Press, 2009.
44 S. B. Piepho and P. N. Schatz *Group Theory in Spectroscopy: with Applications to Magnetic Circular Dichroism*, Wiley-Interscience, 1983, vol. 1.
45 W. R. Mason, *Magnetic Circular Dichroism Spectroscopy*, John Wiley & Sons, 2007.
46 Y. Nam, J. R. Rouxel, J. Y. Lee and S. Mukamel, Monitoring aromatic ring-currents in Mg-porphyrin by time-resolved circular dichroism, *Phys. Chem. Chem. Phys.*, 2020, **22**, 26605–26613.
47 A. D. Becke, Density-Functional Exchange-Energy Approximation with Correct Asymptotic Behavior, *Phys. Rev. A: At., Mol., Opt. Phys.*, 1988, **38**, 3098.

Open Access Article. Published on 03 enero 2022. Downloaded on 20/12/2025 09:30:08 a. m..
This article is licensed under a Creative Commons Attribution-NonCommercial 3.0 Unported Licence.

48 A. D. Becke, Density-Functional Thermochemistry. III. The Role of Exact Exchange, *J. Chem. Phys.*, 1993, **98**, 5648.
49 C. Lee, W. Yang and R. G. Parr, Development of the Colle-Salvetti Correlation-Energy Formula into a Functional of the Electron Density, *Phys. Rev. B: Condens. Matter Mater. Phys.*, 1988, **37**, 785.
50 B. Miehlich, A. Savin, H. Stoll and H. Preuss, Results Obtained with the Correlation Energy Density Functionals of Becke and Lee, Yang and Parr, *Chem. Phys. Lett.*, 1989, **157**, 200–206.
51 M. J. Frisch, *et al.*, *Gaussian 16 Revision A.03*, Gaussian Inc., Wallingford CT, 2016.
52 D. B. Williams-Young, A. Petrone, S. Sun, T. F. Stetina, P. Lestrange, C. E. Hoyer, D. R. Nascimento, L. Koulias, A. Wildman, J. Kasper, J. J. Goings, F. Ding, A. E. DePrince III, E. F. Valeev and X. Li, The Chronus Quantum Software Package, *Wiley Interdiscip. Rev.: Comput. Mol. Sci.*, 2019, e1436.
53 A. D. Bandrauk, E.-W. S. Sedik and C. F. Matta, Effect of absolute laser phase on reaction paths in laser-induced chemical reactions, *J. Chem. Phys.*, 2004, **121**, 7764–7775.
54 P. B. Corkum, N. H. Burnett and F. Brunel, Above-threshold ionization in the long-wavelength limit, *Phys. Rev. Lett.*, 1989, **62**, 1259–1262.
55 S. Sun, D. Williams-Young and X. Li, An Ab Initio Linear Response Method for Computing Magnetic Circular Dichroism Spectra with Nonperturbative Treatment of Magnetic Field, *J. Chem. Theory Comput.*, 2019, **15**, 3162–3169, PMID: 30933558.
56 S. Sun, R. Beck, D. B. Williams-Young and X. Li, Simulating Magnetic Circular Dichroism Spectra with Real-Time Time-Dependent Density Functional Theory in Gauge Including Atomic Orbitals, *J. Chem. Theory Comput.*, 2019, **15**, 6824–6831.
57 S. Sun and X. Li, Relativistic Effects in Magnetic Circular Dichroism: Restricted Magnetic Balance and Temperature Dependence, *J. Chem. Theory Comput.*, 2020, **16**, 4533–4542.
58 K. R. Nandipati and O. Vendrell, On the generation of electronic ring currents under vibronic coupling effects, *J. Chem. Phys.*, 2020, **153**, 224–308.
59 K. Schwennicke and J. Yuen-Zhou, Optical Activity from the Exciton Aharonov–Bohm Effect: A Floquet Engineering Approach, *J. Phys. Chem. C*, 2020, **124**, 4206–4214.
60 H. Mineo, S. Lin and Y. Fujimura, Vibrational effects on UV/Vis laser-driven π-electron ring currents in aromatic ring molecules, *Chem. Phys.*, 2014, **442**, 103–110.
61 J. Yuen-Zhou, S. K. Saikin, N. Y. Yao and A. Aspuru-Guzik, Topologically Protected Excitons in Porphyrin Thin Films, *Nat. Mater.*, 2014, **13**, 1026–1032.

© 2022 The Author(s). Published by the Royal Society of Chemistry